Co-evolution of Viral Processes and Structural Stability in Signed Social Networks

Temirlan Kalimzhanov, Amir Haji Ali Khamseh'i, Aresh Dadlani, *Senior Member, IEEE,*
Muthukrishnan Senthil Kumar, *Member, IEEE,* and Ahmad Khonsari, *Member, IEEE*

Abstract—Prediction and control of spreading processes in social networks (SNs) are closely tied to the underlying connectivity patterns. Contrary to most existing efforts that exclusively focus on positive social user interactions, the impact of contagion processes on the temporal evolution of signed SNs (SSNs) with distinctive friendly (positive) and hostile (negative) relationships yet, remains largely unexplored. In this paper, we study the interplay between social link polarity and propagation of viral phenomena coupled with user alertness. In particular, we propose a novel energy model built on Heider's balance theory that relates the stochastic susceptible-alert-infected-susceptible epidemic dynamical model with the structural balance of SSNs to substantiate the trade-off between social tension and epidemic spread. Moreover, the role of hostile social links in the formation of disjoint friendly clusters of alerted and infected users is analyzed. Using three real-world SSN datasets, we further present a time-efficient algorithm to expedite the energy computation in our Monte-Carlo simulation method and show compelling insights on the effectiveness and rationality of user awareness and initial network settings in reaching structurally balanced local and global network energy states.

Index Terms—Signed networks, epidemic process, balance theory, awareness, continuous-time Markov chain, energy function.

✦

1 INTRODUCTION

QUANTITATIVE analysis of epidemic processes such as infectious diseases, malware codes, and rumors spreading over physical and online social networks (SNs) has stimulated intense research activities [1], [2]. Owing to the pervasive use of social media and the abundance of data extracted from several such networks, which for long were merely unavailable, the theoretical perception of epidemic dynamics driven by nodal interactions has refined substantially in recent years [3], [4]. While the vast majority of research has scrutinized only positive social relationships, user pairs may also signify enmity or distrust as perceived in reality. Subsequently, a user may decisively decline to interact with a hostile contact and avoid involvement in further spread of the viral process [5]. Accounting for heterogeneous social interactions is thus, crucial in characterizing social link valence evolution under the influence of individual user's attitudes towards viral spread.

Unlike conventional networks, signed SNs (SSNs) evolve based on the structural balance theory, pioneered by Heider [6], where the relationship between any two users in a triad (3-clique) can be impacted by the third user [7]. That is to say, the theory posits that if "*the friend of my friend is my friend*" and "*the friend of my enemy is my enemy*", then the resulting triad will be balanced and will constitute an odd number of friendly links. Evidently, SSNs converge to structurally balanced states with minimum social tension by flipping the link polarity to maximize the number of balanced triads [8].

In the jargon of networked epidemics, a handful of works focus on edge sign reconfiguration under the effect of evolving user states. The conditions to attain opinion convergence in generic SNs are obtained in [9] using monotone dynamical systems. Further extended in [10], Shi *et al.* analyze the asymptotic user state evolution affected by deterministic weights on pairwise interactions by formulating a relative-state-flipping model for consensus dynamics in random SSNs and prove the conditions leading to almost sure convergence and divergence. Their analysis assumes that the initial network structure is always balanced which in truth, may not always be the case. Saeedian *et al.* [11] study the non-trivial coupled dynamics over a complete signed graph using an energy function. The authors adopt the susceptible-infected (SI) epidemic model to study the local and global energy minima of the system irrespective of the possibility of recovery to susceptibility or epidemic alertness. Lee *et al.* [12] then introduce an adaptive susceptible-infected-susceptible (SIS) model to reinforce transitivity by rewiring the links between susceptible and infected nodes rather than their signs. Though insightful, the emergent behaviors of the parallel processes in [12] are limited to the population level and do not address the microscopic dynamics inherent in user interactions. Zhang *et al.* [13] present an approximation algorithm for the minimum partial positive influence seeding problem in viral marketing. Moreover, Li *et al.* [14] propose a non-stochastic computational model for maximizing polarity-related linear influence diffusion in SNs. However, neither [13] nor [14] subsume Heider's theory in the network structural evolution.

Thus far, there exists no work that investigates the intriguing co-evolution of generic SN structures and epidemic dynamics of a reversible process in conjunction with user alertness. Absent in classical epidemic models, *awareness* towards viral processes is an intrinsic human response that plays the role of a natural immunization strategy. Such change in hu-

• *T. Kalimzhanov and A. Dadlani are with the Department of Electrical and Computer Engineering, Nazarbayev University (NU), Nursultan 010000, Kazakhstan. E-mails: {temirlan.kalimzhanov, aresh.dadlani}@nu.edu.kz*
• *A. H. A. Khamseh'i and A. Khonsari are with the School of Electrical and Computer Engineering, College of Engineering, University of Tehran, Tehran 1439957131, Iran. E-mails: {khamse, a_khonsari}@ut.ac.ir*
• *M. S. Kumar is with the Department of Applied Mathematics and Computational Sciences, PSG College of Technology, Coimbatore 641004, India. E-mail: msk.amcs@psgtech.ac.in*

Fig. 1. Schematic of the SAIS spreading model over an SN with positive (solid) and negative (dashed) social relationships.

Fig. 2. All possible pairwise links in the SAIS spreading model. The edges enclosed in boxes are the only two transmissible configurations.

man behavior can be induced by learning about the contagion spread from others without having to encounter it firsthand. This hence, results in a coupled situation where an infectious person and information about its presence spread simultaneously when humans react to the presence of the infection. In fact, raising awareness is a widely-practiced control strategy in dynamical systems as it alters the progression of the viral spread [15], [16]. Besides the analytical merits, such a refined projection model may serve beneficial to network administrators, social influencers, and decision makers in devising optimal resource allocation policies. In view of this research gap, the main contributions of this work are as follows:

- Inspired by Heider's balance theory, a novel energy-based framework is proposed to jointly minimize the number of unbalanced triads that contribute to the social tension while mitigating the viral spread in SNs. To capture users' response to such processes, we formulate the susceptible-alert-infected-susceptible (SAIS) epidemic model [15] as a continuous-time Markov chain (CTMC) and derive the stationary probabilities to investigate the virtues of promoting awareness on the network structural evolution.
- By incorporating a tuning parameter, we then analyze cases for which the initial fraction of positive links and the initially infected users induce *natural immunization* by segregating the alerted and infected users into two clusters interconnected via unfriendly links.
- Our model is evaluated on three real SSN datasets by employing a time-efficient Monte Carlo simulation method under different parametric settings.

2 THE COUPLED NETWORK MODEL

In this section, we first formulate the stochastic SAIS model re-purposed for general spreading processes in our analysis. The proposed energy model is then detailed subsequently.

2.1 Stochastic Epidemic Model Description

We consider an undirected SSN, represented by the graph $\mathcal{G}_t = (\mathcal{V}, \mathcal{E}_t)$, with a set $\mathcal{V} = \{1, 2, \ldots, n\}$ of n users that form friendly (1), hostile (-1), or no (0) social links. The link polarity of user pair $(i, j) \in \mathcal{E}_t$ at any given time t is denoted by $\mathcal{A}_{i,j}(t) \in \{-1, 0, 1\}$ [11]. For epidemic spreading over $\mathcal{G}_t$, the SAIS model in Fig. 1 is used, where each user is in the susceptible (S), alert (A), or infected (I) state at time t. User i is said to be susceptible if he/she is completely unaware of the spreading process. Since these processes do not propagate over negative links in SNs [17], a susceptible user gets infected with rate $\beta \in \mathbb{R}^+$ times the number of its infected friendly contacts [15]. A user aware of the process however, is less likely to get infected, with a lower infection rate $0 \leq \beta_a < \beta$, as compared to a susceptible user. Unlike the irreversible SI model in [11], a susceptible user becomes aware of the process with rate
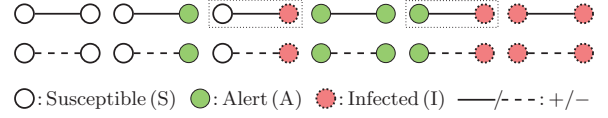
$\kappa \in \mathbb{R}^+$ times the number of direct infected friends and all infected users may eventually recover back to susceptibility with rate $\delta \in \mathbb{R}^+$. For all $i \in \mathcal{V}$, the network state can thus, be expressed formally as the CTMC $\{X_i(t); t \geq 0\}$, where:

$$X_i(t) = \begin{cases} 1; & \text{if user } i \text{ is susceptible at time } t, \\ 0; & \text{if user } i \text{ is alert at time } t, \\ -1; & \text{if user } i \text{ is infected at time } t. \end{cases} \quad (1)$$

Using (1), we now can define the probability of user i being in one of the three epidemic states as $S_i(t) = \Pr[X_i(t) = 1]$, $A_i(t) = \Pr[X_i(t) = 0]$, and $I_i(t) = \Pr[X_i(t) = -1]$ such that for $1 \leq i \leq n$, $S_i(t) + A_i(t) + I_i(t) = 1$ always holds.

2.2 Pairwise Spreading Energy Function

We now delineate the sign evolution of user interactions in the context of energy. Given the three epidemic states (S, A, I) and binary link signs ($-, +$), there exist 12 distinct user pair configurations as shown in Fig. 2. We characterize the viral potency by mapping each user pair configuration (i, j), where $i, j \in \mathcal{V}$, to the energy landscape as follows:

$$E_{i,j}^p(t) \triangleq \begin{cases} \mathcal{A}_{i,j}(t) \frac{\left(X_i(t) - X_j(t)\right)^2}{4}; & \text{if } |X_i + X_j| \bmod 2 = 0, \\ \mathcal{A}_{i,j}(t) \frac{1 - X_i(t) - X_j(t)}{2}; & \text{otherwise.} \end{cases} \quad (2)$$

Based on the functional value of (2), the configurations depicted in Fig. 2 can be classified as follows:

- *Balanced edges:* As long as configurations $S - I$ and $A - I$ do not flip their edge signs while evolving, the users i and j are in a balanced social relationship and do not engage in the propagation process [11]. Therefore, they exhibit a pairwise energy of $E_{i,j}^p(t) = -1$.
- *Unbalanced edges:* Cases in which a susceptible or alert user is in a friendly relationship with an infected user are socially unstable and are bound to change with time. In our model, $S + I$ and $A + I$ serve as feasible links for epidemic spread and thus, the users are in an unbalanced state with pairwise energy of $E_{i,j}^p(t) = 1$.
- *Neutral edges:* Irrespective of the edge sign, configurations $S \pm S$, $I \pm I$, $A \pm A$, and $S \pm A$ do not contribute to the spreading process, and thus, exhibit zero pairwise energy, i.e., $E_{i,j}^p(t) = 0$.

Accordingly, the total pairwise spreading energy of network $\mathcal{G}_t$, denoted by $E_p(\mathcal{G}_t)$, can be computed as:

$$E_p(\mathcal{G}_t) = \frac{1}{\binom{n}{2}} \sum_{\substack{i,j \\ i \neq j}} E_{i,j}^p(t). \quad (3)$$

2.3 Triad Structural Energy Function

Along with the users' epidemic states, edge sign evolution is also driven by Heider's structural balance criterion. A triad of users in $\mathcal{G}_t$, denoted by (i, j, k), is said to be balanced if the product of $\mathcal{A}_{i,j}(t) \cdot \mathcal{A}_{j,k}(t) \cdot \mathcal{A}_{k,i}(t)$ is positive. In other words, an unbalanced triad will always have an odd number of negative edges. Hence, network $\mathcal{G}_t$ is *fully* balanced only if all
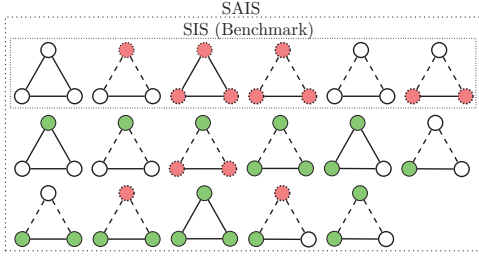
Fig. 3. All possible balanced triads in the SAIS and the SIS models.

Fig. 4. Transition probabilities for temporal evolution of states in Fig. 2.

the constituent triads are balanced. Conforming to Heider's balance theory, the structural status of any triad (i, j, k) can be mapped to the energy landscape as below [6]:

$$E^{\blacktriangle}_{i,j,k}(t) \triangleq -\mathcal{A}_{i,j}(t) \cdot \mathcal{A}_{j,k}(t) \cdot \mathcal{A}_{k,i}(t). \qquad (4)$$

With (4) in place, the energy contribution of any balanced (unbalanced) triad in $\mathcal{G}_t$ is $E^{\blacktriangle}_{i,j,k}(t) = -1$ ($E^{\blacktriangle}_{i,j,k}(t) = 1$). Fig. 3 showcases all the balanced triads for the SAIS and the SIS (baseline) models. To converge towards lower energy states (which corresponds to more social stability), users in unbalanced triads tend to flip their link signs which in turn, affects the configuration of other triads that share common edges with them. Consequently, the total normalized energy of $\mathcal{G}_t$, denoted by $E_\triangle(\mathcal{G}_t)$, is as follows, where $-1 \leq E_\triangle(\mathcal{G}_t) \leq 1$:

$$E_\triangle(\mathcal{G}_t) = \frac{1}{\binom{n}{3}} \sum_{\substack{i,j,k \\ i \neq j \neq k}} E^{\blacktriangle}_{i,j,k}(t), \qquad (5)$$

Users in triads decide on whether or not to alter their relationships only if the total triad energy of the resulting network is further reduced. Apparently, SNs that manifest triad energy values closer to -1 tend to be socially more stable and thus, pragmatically justified.

2.4 Weighted Network Energy Function

We now define the total energy of network $\mathcal{G}_t$, given by $E(\mathcal{G}_t)$, as the weighted sum of the overall pairwise and triad energy functions derived in (3) and (5), respectively:

$$E(\mathcal{G}_t) = \alpha \cdot E_\triangle(\mathcal{G}_t) + (1 - \alpha) \cdot E_p(\mathcal{G}_t), \qquad (6)$$

where $\alpha (0 \leq \alpha \leq 1)$ is the tuning parameter used to adjust the energy trade-off between the epidemic spread ($\alpha = 0$) and the structural balance ($\alpha = 1$) in the network. Hence, if $\mathcal{G}_t$ is fully balanced (fully unbalanced), then $E(\mathcal{G}_t) = -1$ ($E(\mathcal{G}_t) = 1$), which is more likely to be achieved in smaller graphs. Note that for some fixed α value, attaining the global (local) energy minimum state in which $\mathcal{G}_t$ is fully (or nearly) balanced depends on the initial fractions of infected users ($0 \leq \rho_0 \leq 1$) and friendly links ($0 \leq r_0 \leq 1$) [11].

3 STEADY-STATE PROBABILITY DISTRIBUTION

Assuming that only one event is triggered in each time step, $\Delta t \ll 1$, i.e., either the epidemic state of exactly one user pair (i, j) changes or the edge sign is flipped, the rules defining the user pair transitions are shown in Fig. 4. The balanced edges S−I and A−I transition to S−S and A−S, respectively, with probability $\delta \cdot \Delta t$ or change to S+I and A+I, respectively, with probability $1 - \delta \cdot \Delta t$. For unbalanced edges, S+I changes to S−I with probability $1 - \delta \cdot \Delta t - (\beta + \kappa) \cdot \Delta t \cdot (1 - 2\delta \cdot \Delta t)$ or switches to states A+I, I+I, or S+S with probabilities $\kappa \cdot \Delta t (1 - \delta \cdot \Delta t), \beta \cdot \Delta t (1 - \delta \cdot \Delta t),$ and $\delta \cdot \Delta t (1 - (\beta + \kappa) \cdot \Delta t),$
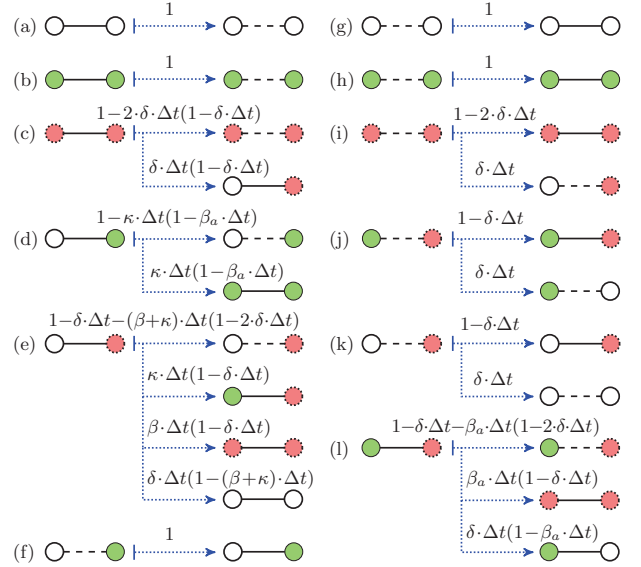
respectively. Also, A+I switches to A−I, I+I, or A+I with probabilities $1 - \delta \cdot \Delta t - \beta_a \cdot \Delta t \cdot (1 - 2\delta \cdot \Delta t), \beta_a \cdot \Delta t (1 - \delta \cdot \Delta t),$ and $\delta \cdot \Delta t (1 - \beta_a \cdot \Delta t),$ respectively. Among the neutral edges, S±S, A±A, and S−A flip their edge signs with probability 1 in each time step, S+A changes to either S−A or A+A with probabilities $1 - \kappa \cdot \Delta t \cdot (1 - \beta_a \cdot \Delta t)$ and $\kappa \cdot \Delta t \cdot (1 - \beta_a \cdot \Delta t),$ respectively. Finally, I±I changes to I∓I with probabilities $1 - 2\delta \cdot \Delta t \cdot (1 - \delta \cdot \Delta t)$ and $1 - 2\delta \cdot \Delta t,$ respectively, and to S⊞H with probabilities $\delta \cdot \Delta t \cdot (1 - \delta \cdot \Delta t)$ and $\delta \cdot \Delta t,$ respectively.

In general, given the pair (i, j), the tri-variate CTMC of the form $\{Z_{i,j}(t); t \geq 0\}$, where $Z_{i,j}(t) = (X_i(t), X_j(t), \mathcal{A}_{i,j}(t))$, defines these conditional transition probabilities as follows:

$$\mathcal{P}_{c,c'}(\Delta t) \triangleq \Pr \Big[Z_{i,j}(t + \Delta t) = c' \big| Z_{i,j}(t) = c \Big], \qquad (7)$$

where $c = (x, y, z)$, $c' = (x', y', z')$, and $x, y, z, x', y', z' \in \{-1, 0, 1\}$. Based on (7), the stead-state probability distribution is derived in Theorem 1.

Theorem 1. Let $\{\pi_{x,y,z} | x, y, z \in \{-1, 0, 1\}\}$ be the stationary probabilities for the CTMC $Z_{i,j}(t)$ defined above, then we have the following in steady-state:

(i) The fraction of susceptible users (s_∞) is $\sum_{y,z} \pi_{1,y,z}$.
(ii) The fraction of infected users (ρ_∞) is $\sum_{y,z} \pi_{-1,y,z}$.
(iii) The fraction of alerted users (a_∞) is $\sum_{y,z} \pi_{0,y,z}$.
(iv) The fraction of friendly links (r_∞) is $\sum_{x,y} \pi_{x,y,1}$.

Proof. We use (7) to obtain the elements of the infinitesimal generator matrix $Q = [q_{c,c'}]$ of order 27 as follows:

$$q_{c,c'} = \begin{cases} \lim_{\Delta t \to 0} \frac{\mathcal{P}_{c,c'}(\Delta t) - 1}{\Delta t}; & \text{if } c' = c, \\ \lim_{\Delta t \to 0} \mathcal{P}_{c,c'}(\Delta t); & \text{if } c' \neq c. \end{cases} \qquad (8)$$

From (8), we now can obtain the stationary probabilities by solving $\Pi \cdot Q = 0$ and $\Pi \cdot \mathbf{1} = 1$, where $\Pi = \{\pi_{x,y,z} | x, y, z \in \{-1, 0, 1\}\}$. Denoted by $s_\infty = \sum_{i=1}^n S_i(\infty) / |\mathcal{V}|$, the fraction of susceptible users is computed as:

$$s_\infty = \sum_{y,z} \pi_{1,y,z}.$$

Similarly, the steady-state probabilities for ρ_∞, a_∞, and r_∞ can be obtained straightforwardly. □

Algorithm 1 Time-efficient Network Energy Calculation

Input: $\mathcal{G}_0 = (\mathcal{V}, \mathcal{E}_0)$, α, ρ_0, r_0, β, β_a, κ, and δ.
Output: $E_{min}(\mathcal{G})$.
   Initialization: $\forall (i,j), \mathcal{A}_{i,j}(0) \in \mathcal{E}_0 = -1$, and $e = 1$.
 1: Calculate $E(\mathcal{G}_0)$ using (6).
 2: $e \leftarrow E(\mathcal{G}_0)$.
 3: **for** $t \leftarrow \Delta t$ to $T \cdot \Delta t$ **do**
 4:    Randomly select an edge $(i,j) \in \mathcal{E}_{t-\Delta t}$.
 5:    Change the state of edge (i,j) according to Fig. 4.
 6:    Update $E(\mathcal{G}_t)$ using (9), (11), and (12).
 7:    **if** $E(\mathcal{G}_t) == e$ **then**
 8:      $e \leftarrow E(\mathcal{G}_t)$ with probability 0.5.
 9:    **else if** $E(\mathcal{G}_t) < e$ **then**
10:      $e \leftarrow E(\mathcal{G}_t)$
11: **return** $E_{min}(\mathcal{G}) \leftarrow e$

---

4 MONTE CARLO METHOD

Starting from an initial network state at $t = 0$, where a fraction of users (ρ_0) are randomly infected, we select an edge (i, j) at random in each evolution step of the simulation and change its state as in Fig. 4. Doing so affects the energy states of all triads that share edge (i, j) in the long-term which successively, alters the total network energy state. Convergence towards the new network structure transpires as long as the new energy state decreases in each time step [11], i.e., this process continues until the global minimum $(E(\mathcal{G}_t) = -1)$ or a local $(E(\mathcal{G}_t) > -1)$ minimum energy state is reached. Computing $E(\mathcal{G}_t)$ using (6) in each time step takes $O\left(\binom{n}{2} + \binom{n}{3}\right)$ time. To expedite the computation, we propose Algorithm 1 that evaluates the energy difference of the selected edge between consecutive time steps, t' and t'' $(t'' = t' + \Delta t)$, in $O(1)$ time as:

$$\Delta E(i,j) = \alpha \cdot \Delta E_\triangle(i,j) + (1-\alpha) \cdot \Delta E_p(i,j), \quad (9)$$

where $\Delta E_\triangle(i,j)$ is the difference in the triad energy, i.e.,

$$\Delta E_\triangle(i,j) = \frac{1}{\binom{n}{3}} \sum_{i',j',k'} \left(E^\blacktriangle_{i',j',k'}(t'') - E^\blacktriangle_{i',j',k'}(t') \right)$$

$$= \frac{\mathcal{A}_{i,j}(t') - \mathcal{A}_{i,j}(t'')}{\binom{n}{3}} \sum_{k' \neq i,j} \mathcal{A}_{i,k'}(t') \cdot \mathcal{A}_{j,k'}(t'). \quad (10)$$

If the state transition does not flip the edge sign, then $E_\triangle(\mathcal{G}_t)$ remains unaltered. Otherwise, flipping the edge sign implies that $\mathcal{A}_{i,j}(t'') = -\mathcal{A}_{i,j}(t')$, which further reduces (10) to:

$$\begin{cases} \frac{-2\mathcal{A}_{i,j}(t'')}{\binom{n}{3}} \sum_{k' \neq i,j} \mathcal{A}_{i,k'}(t') \cdot \mathcal{A}_{j,k'}(t'); & \text{if } \mathcal{A}_{i,j}(t'') = -\mathcal{A}_{i,j}(t'), \\ 0; & \text{if } \mathcal{A}_{i,j}(t'') = \mathcal{A}_{i,j}(t'). \end{cases} \quad (11)$$

Similarly, $\Delta E_p(i,j)$ can be computed as follows:

$$\Delta E_p(i,j) = \frac{1}{\binom{n}{2}} \left(E^p_{i,j}(t'') - E^p_{i,j}(t') \right). \quad (12)$$

5 SIMULATION RESULTS AND DISCUSSIONS

We evaluate the proposed energy framework with respect to r_0, ρ_0, and α. For Case Study I, we generate a complete network of $|\mathcal{V}| = 180$ users to entail the maximum number of triads in our analysis. We then apply the bootstrap technique to extract i.i.d. samples of smaller connected components of size $|\mathcal{V}|$ from the Slashdot081106 (SL, $|\mathcal{V}| = 747$) [18] and the Bitcoin-OTC (BC, $|\mathcal{V}| = 709$) [18] datasets, and the entire US Congress co-sponsorship (CS, $|\mathcal{V}| = 100$, $|\mathcal{E}_t| = 3696$) [19] dataset in Case Study II. To ensure better theoretical predictions, all Monte Carlo simulation results are averaged over
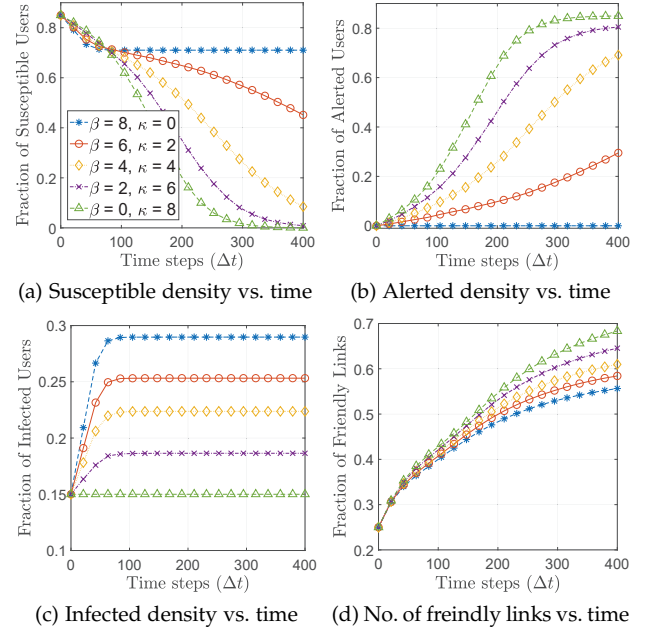

(a) Susceptible density vs. time   (b) Alerted density vs. time

(c) Infected density vs. time   (d) No. of freindly links vs. time

Fig. 5. Time evolution of the proposed spreading model for different (β, κ) values. The SIS baseline model is traced as $(\beta = 8, \kappa = 0)$.

100 runs on a PC with 3.2 GHz Intel Core i9-9900 CPU and 16 GB RAM[1].

5.1 Case Study I: Results

For the synthetic network, Fig. 5 plots the trajectories for a viral outbreak under varying (β, κ) values with $r_0 = 0.25$, $p_0 = 0.15$, $\alpha = 0.5$, $\beta_a = 0.3\beta$, and $\delta = 9$ [15], [16]. As shown in Fig. 5a, unlike the SIS baseline $(\kappa = 0)$, the susceptible fraction under the SAIS model drops to zero with rate proportional to κ. As a result, the users are either influenced by the viral process or alerted thus making them less likely to fall prey in the long run since $\beta_a \ll \beta$. The impact of κ on the alerted and infected user densities are, respectively, shown in Fig. 5b and Fig. 5c. For higher κ values, a larger susceptible fraction is made aware of the spread which, in turn, diminishes the size of the infected population. For instance, in contrast to the baseline, Fig. 5c vividly shows that the infected cluster size decreases by nearly 14% when $\kappa = 2$. In spite of setting $\beta = 0$, note that there exists a non-zero infected population in the network. This clearly implies that for smaller values of r_0, the proposed model partitions the network into two distinct clusters: one comprising of alerted users and the other containing infected users. While the users within each cluster maintain a friendly relationship with each other, they are hostile towards users in the other cluster. The virality of the process however, dies out gradually with rise in r_0 and the two clusters eventually merge into a single cluster of alert users. The impact of κ on the number of friendly links is shown in Fig. 5d. Driven by the transitions given in Fig. 4, such behavior is not far from expectation as users are inclined to detach from friends influenced by the spreading phenomena and instead, befriend those who are informed or share common interests to attain social stability.

Fig. 6 shows how the control parameter α arbitrates the epidemic spread and social tension trade-off for varying r_0

(a) ρ_∞ vs. (α, r_0) (b) $E(\mathcal{G})$ vs. (α, r_0)
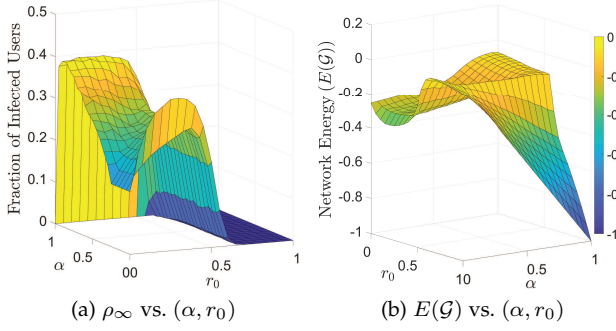
Fig. 6. Impact of α and r_0 on the steady-state infection density and the network energy for $p_0 = 0.15$, $\beta = 6$, $\kappa = 4$, $\beta_a = 0.3\beta$, and $\delta = 9$.

(a) ρ_∞ vs. (ρ_0, r_0) (b) $E(\mathcal{G})$ vs. (ρ_0, r_0)

Fig. 7. Impact of ρ_0 and r_0 on the steady-state infection density and the network energy for $\alpha = 0.5$, $\beta = 6$, $\kappa = 4$, $\beta_a = 0.3\beta$, and $\delta = 9$.
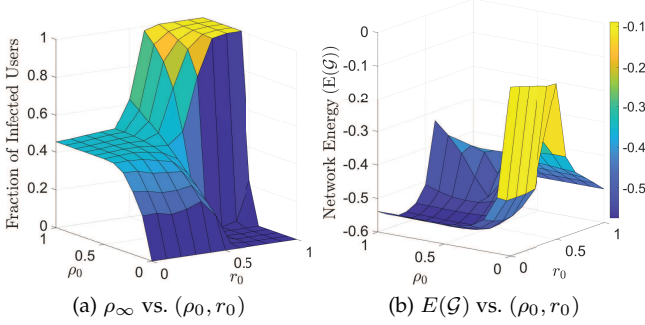
values in steady-state. In Fig. 6a, we observe that the system gravitates towards the jammed states ($E(\mathcal{G}) < -1$), where mitigating the epidemic is favored over attaining structural balance, for lower (α, r_0) values. As α and r_0 goes beyond 0.5 however, it is evident in Fig. 6b that the network tends towards the global minimum energy state to become structurally robust at the expense of further epidemic spread. Interestingly, due to the reversible nature of the SAIS model, the fully balanced complete network progresses to be infection-free at $\alpha = r_0 = 1$ as all users eventually become aware of the spread. Hence, the network tends to exploit the negative links to naturally immunize the susceptible users by separating them from the cluster of infected users. Therefore, for any given setting, an optimal (α, r_0) pair exists for which the network would contain minimum number of infected users in steady-state and yet, not necessarily be socially balanced.

The significance of ρ_0 in the coupled evolution is shown in Fig. 7. For $0 \leq \rho_0, r_0 \leq 0.5$, Fig. 7a showcases the impact of negative links in controlling the contagious spread. Further increase in ρ_0 however, yields a fixed fraction of infected users as most of the triads have evolved into a balanced state. Full recovery is attained when $\rho_0 \leq 0.5$ and $r_0 > 0.5$ due to the small infection prevalence and the low infection rate relative to κ and δ. Also, note that for low ρ_0, the stationary infection density (ρ_∞) drops to zero, irrespective of r_0. The process diffuses at its maximum when ρ_0 and r_0 are both high. Fig. 7b shows the trivial effect of ρ_0 on the net network energy for high r_0, where the triad structural energy is dominant. Around $r_0 = 0.5$, the network struggles to become balanced as flipping the edge sign conceivably creates more unbalanced triads as compared to other values on the r_0 spectrum. Fig. 8 shows $E_p(\mathcal{G})$ and $E_\triangle(\mathcal{G})$ against r_0 for different (β, κ) values in steady-state. As seen in Fig. 8a, the minimum achievable pairwise and triad energy values increase with κ for $r_0 < 0.6$,
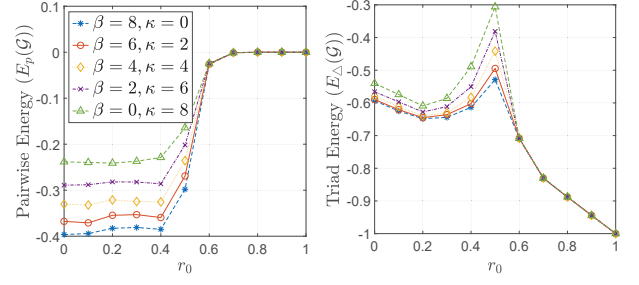

(a) Pairwise energy vs. r_0 (b) Triad energy vs. r_0

Fig. 8. Minimum pairwise and triad energy for different (β, κ) values. Here, $p_0 = 0.15$, $\alpha = 0.5$, $\beta_a = 0.3\beta$, and $\delta = 9$.

TABLE 1
Performance under network scalability for $\rho_0 = 0.15$ and $(\beta, \kappa) = (4, 4)$

	$|\mathcal{V}|$	Density	ρ_∞	a_∞	r_∞	$|\triangle_B|$
SL	200	$\approx 4.37\%$	0.22	0.32	0.43	0.987
	498	$\approx 1.20\%$	0.16	0.16	0.38	0.993
	747	$\approx 1.10\%$	0.17	0.11	0.37	0.936
BC	161	$\approx 4.25\%$	0.22	0.39	0.41	0.984
	460	$\approx 1.46\%$	0.193	0.19	0.39	0.928
	709	$\approx 0.93\%$	0.17	0.11	0.38	0.906
CS	100	$\approx 74.67\%$	0.21	0.79	0.66	0.993

whereas the ρ_∞ inversely drops. But for larger r_0, the impact of β and κ on the energy and ρ_∞ is minimal. That is to say, $E_p(\mathcal{G})$ in Fig. 8a increases to zero as the number of infected users becoming aware rapidly grows with increase in friendly links. Contrarily, $E_\triangle(\mathcal{G})$ in Fig. 8b falls to the global energy minimum because the triads gradually evolve to become socially stable as most users have already formed friendly links.

5.2 Case Study II: Results

We now assess our model using the real sparsely-connected SL ($\approx 1.10\%$), BC ($\approx 0.93\%$), and the dense CS ($\approx 74.67\%$) SN datasets. The total number of triads existing in SL, BC, and CS are 4268, 1588, and 74140, respectively[2]. Table 1 compares the impact of network scalability on the model performance.

Fig. 9 depicts the steady-state results of the datasets with respect to generic β and κ values. Consistent with Fig. 6a and Fig. 7a, we see in Fig. 9a that ρ_∞ reduces with rise in awareness for $\rho_0 = 0.15$, while it remains high and almost the same for $\rho_0 = 0.75$. As a resultant, the fraction of alerted users increases with κ as shown in Fig. 9b. It is noteworthy that, irrespective of ρ_0, the gap in a_∞ between CS and the other two datasets gradually decreases. Despite the fewer nodes in CS, the plots reveal the profound impact of κ on the nodal states of densely connected CS that contains more number of triads. Summing up the infected and alerted fractions for each (β, κ) pair also justifies the natural immunization induced by the formation of two-cluster networks. Changes in β and κ however, do not seem to influence the fraction of friendly links (r_∞) in steady-state. Though the epidemic state of nodes are decisive in link sign evolution, we see that for all scenarios the ultimate number of friendly ties is almost the same. Upon reaching steady-state, the fraction of balanced triads, denoted by $|\triangle_B|$, is close to 100% in Fig. 9d, which indicates a balanced SN structure in accordance with Heider's balance theory. Furthermore, the results empirically show that although the structural energy

2. In general, the sharp upper bound on the number of triads in a graph with n nodes and m edges is $\frac{n}{6}(2m - n + 1)^{3/2}$.
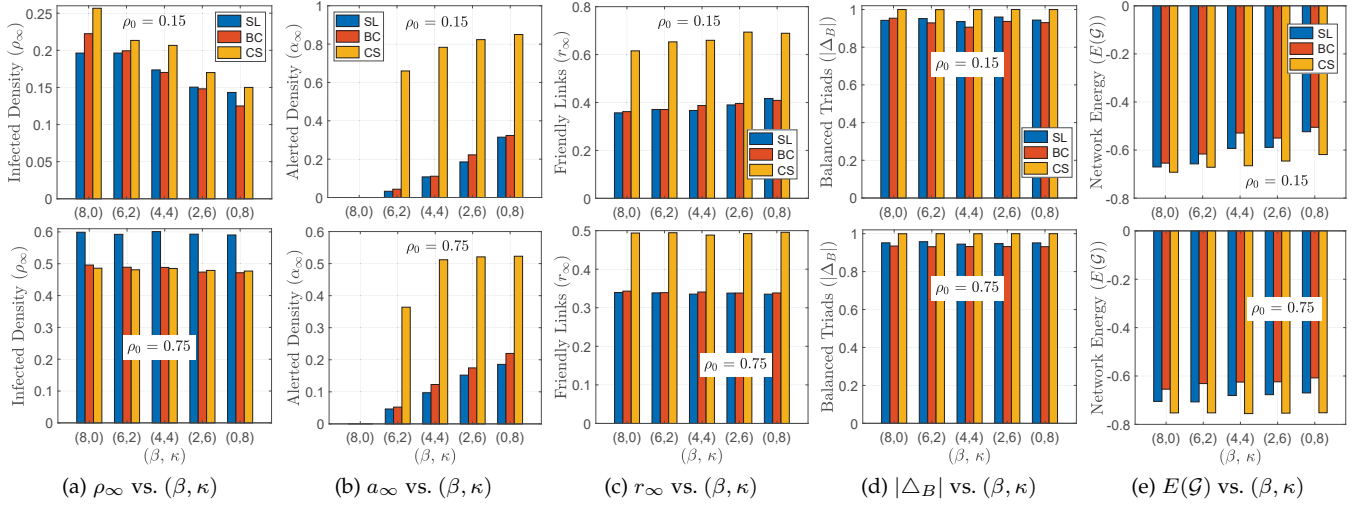
Fig. 9. Experimental results on SL, BC, and CS for varying (β, κ) values. Here, $r_0 = 0.25$, $p_0 = \{0.15, 0.75\}$, $\alpha = 0.5$, $\beta_a = 0.3\beta$, and $\delta = 9$.

of triads approach a global minimum, $E(\mathcal{G})$ does not reach the global energy minimum state. This is because the pairwise energy tends towards a local energy minimum state when $\alpha = 0.5$. Also, since κ affects the pairwise spreading energy, $E(\mathcal{G})$ is slightly lower for higher κ rates as plotted in Fig. 9e. Comparing the trends in both rows of Fig. 9, the results for r_∞ and $|\triangle_B|$ are almost alike. With increase in κ, $E(\mathcal{G})$ of CS is higher by roughly 28% for $\rho_0 = 0.15$ because of the larger population of alerted users being intrinsically immunized as compared to the setting with $\rho_0 = 0.75$, where the impact of increasing κ is relatively inconsequential.

6 CONCLUSION

In this paper, coupled dynamics of the SAIS epidemic model and the structural evolution of SSNs was studied. Inspired by Heider's balance theory, a network energy framework was formulated to capture the viral spreading via pairwise user interactions in conjunction with social stability in triad configurations. The superiority of incorporating user awareness in the classical SIS model was fully validated by the Monte Carlo simulation results. Moreover, it was shown that a complete SSN splits into two clusters of alerted and infected users upon reaching a local energy minimum. The alerted cluster density was also found to grow with increase in the initial number of friendly links and a fully balanced SSN becomes infection-free only when the triad energy is considered and all initial user links are friendly. One interesting future work is to leverage network centrality measures other than degree distribution in probing the trade-off between opposing epidemics and social stability in directed and composite SSNs. Better parameter estimations based on network spectral analysis is also of value in adopting effective control strategies.

REFERENCES

[1] T. Britton, "Epidemic models on social networks—with inference," *Statistica Neerlandica*, vol. 74, no. 3, pp. 222–241, Feb. 2020.
[2] D.-W. Huang, L.-X. Yang, P. Li, X. Yang, and Y. Y. Tang, "Developing cost-effective rumor-refuting strategy through game-theoretic approach," *IEEE Syst. J.*, pp. 1–12, Sep. 2020.
[3] A. Dabarov, M. Sharipov, A. Dadlani, M. S. Kumar, W. Saad, and C. S. Hong, "Heterogeneous projection of disruptive malware prevalence in mobile social networks," *IEEE Commun. Lett.*, vol. 24, no. 8, pp. 1673–1677, Aug. 2020.
[4] H. Shafiei, A. Khonsari, S. Kashipazha, and A. Dadlani, "The tongue can paint: Understanding popularity in podcasting societies," in *Proc. ACM Web Conference*, Apr. 2020.
[5] J. Leskovec, D. Huttenlocher, and J. Kleinberg, "Signed networks in social media," in *Proc. ACM SIGCHI Conf. Human Factors Comput. Syst.*, 2010, pp. 1361–1370.
[6] F. Heider, *The psychology of interpersonal relations*. Hoboken, NJ, US: John Wiley & Sons Inc, 1958.
[7] R. Sun, C. Chen, X. Wang, Y. Zhang, and X. Wang, "Stable community detection in signed social networks," *IEEE Trans. Knowl. Data Eng.*, pp. 1–1, 2020.
[8] L. Hedayatifar, F. Hassanibesheli, A. Shirazi, S.V. Farahani, and G. Jafari, "Pseudo paths towards minimum energy states in network dynamics," *Physica A*, vol. 483, pp. 109–116, Oct. 2017.
[9] C. Altafini, "Consensus problems on networks with antagonistic interactions," *IEEE Trans. Autom. Control*, vol. 58, no. 4, pp. 935–946, Apr. 2013.
[10] G. Shi, A. Proutiere, M. Johansson, J. S. Baras, and K. H. Johansson, "Emergent behaviors over signed random dynamical networks: State-flipping model," *IEEE Trans. Control Netw. Syst.*, vol. 2, no. 2, pp. 142–153, Jun. 2015.
[11] M. Saeedian, N. Azimi-Tafreshi, G. R. Jafari, and J. Kertesz, "Epidemic spreading on evolving signed networks," *Phys. Rev. E*, vol. 95, p. 022314, Feb. 2017.
[12] H.-W. Lee, N. Malik, F. Shi, and P. J. Mucha, "Social clustering in epidemic spread on coevolving networks," *Physical Review E*, vol. 99, no. 6, Jun. 2019.
[13] Z. Zhang, Y. Shi, J. Willson, D.-Z. Du, and G. Tong, "Viral marketing with positive influence," in *Proc. IEEE Conf. on Comp. Commun. (INFOCOM)*, 2017, pp. 1–8.
[14] D. Li and J. Liu, "Modeling influence diffusion over signed social networks," *IEEE Trans. Knowl. Data Eng.*, vol. 33, no. 2, pp. 613–625, Feb. 2021.
[15] F. Darabi Sahneh and C. Scoglio, "Epidemic spread in human networks," in *Proc. IEEE Conf. Decis. Control and Eur. Control Conf. (CDC-ECC)*, 2011, pp. 3008–3013.
[16] F. D. Sahneh, A. Vajdi, J. Melander, and C. M. Scoglio, "Contact adaption during epidemics: A multilayer network formulation approach," *IEEE Trans. Netw. Sci. Eng.*, vol. 6, no. 1, pp. 16–30, Jan. 2019.
[17] J. Tang, Y. Chang, C. Aggarwal, and H. Liu, "A survey of signed network mining in social media," *ACM Comput. Surv.*, vol. 49, no. 3, pp. 1–37, Dec. 2016.
[18] J. Leskovec and A. Krevl, "SNAP Datasets: Stanford large network dataset collection," http://snap.stanford.edu/data, Jun. 2014.
[19] Z. Neal, "A Sign of the Times: Dataset of US Congress signed network backbones from co-sponsorship data, 1973-2016," Jan. 2020. [Online]. Available: https://doi.org/10.6084/m9.figshare.8096429.v3